Chalcogenide Letters Vol. 21, No. 7, July 2024, p. 575 - 581

Effects of thermal and laser annealing on the structure of $Ge_2Sb_2Te_5$ thin films

K. Turmanova[a], O. Prikhodko[a], Zh. Tolepov[a], S. Maksimova[a], N. Manabaev[b], N. Almas[c,*]
[a]*NAO al-Farabi Kazakh National University, 71 Al-Farabi Avn, IETP, 050040 Almaty, Kazakhstan*
[b]*Department of General Physics, Satbayev University, Satpayeva st., 22, 050040 Almaty, Kazakhstan*
[c]*Department of Science and Innovation, Astana IT University, Mangilik Yel Avn, 55/11, 010000 Astana, Kazakhstan*

In this study, we used Raman spectroscopy to compare the local structure of Ge2Sb2Te5 (GST) thin films with thicknesses of 90 nm and 271 nm that were crystallized through thermal annealing and laser radiation (laser annealing) during the recording of Raman spectra in situ. We found that for all crystallized films, the position of the main peaks in the Raman spectra was almost the same, and their structure corresponded to a hexagonal close packed state. It is noteworthy that the full width at half maximum (FWHM) of the main peaks varies considerably depending on the crystallization method used.

(Received April 28, 2024; Accepted July 24, 2024)

Keywords: Amorphous semiconductor, Sputtering, GST, Raman spectroscopy, FWHM

1. Introduction

Alloys within the Ge-Sb-Te system, notably the Ge2Sb2Te5 (GST) compound, are garnering increased interest due to their potential application in the development of advanced non-volatile phase change random access memory (PCRAM) cells for both micro- and nanoelectronics [1]. PCRAM cells stand out as promising candidates for next-generation memory devices, poised to replace existing memory technologies [2,3].

These devices operate on the principle of swiftly altering the optical and electrical characteristics of chalcogenide material during a phase transition between its amorphous and crystalline states [4-6]. This transition is triggered in chalcogenide semiconductors either by laser irradiation or through the application of an electrical pulse. Rapid heating above the melting point followed by quick cooling induces the amorphous state, whereas sustained heating just below the melting point restores the crystalline structure. The reliability of phase change memory (PCM) devices hinges largely on the stability of the properties of the chalcogenide semiconductor employed. It's projected that PCM will offer significantly enhanced reliability in terms of both information storage durability and cyclability, compared to flash memory. However, this aspect hasn't been thoroughly explored, as evidenced by the wide range in estimated data for PCM devices [7,8]. This variability may stem from numerous influencing factors on PCM reliability [9-16].

The crystallinity degree of GST film structures holds significant importance in this context. Film crystallization can be achieved via thermal annealing or laser irradiation methods. Raman spectroscopy serves as a pivotal tool for monitoring the transition between amorphous and crystalline states, particularly when film thickness exceeds the limits of transmission electron microscopy (TEM) (>50-70 nm) and falls below those of X-ray diffraction (XRD) (<400 nm). In the case of studying the structural changes induced by laser irradiation, in situ Raman spectroscopy is employed to gradually crystallize amorphous films while continuously recording spectra until a stable crystalline state is attained. The extent of similarity between the crystal structures of films

* Corresponding author: n.almas@astanait.edu.kz
https://doi.org/10.15251/CL.2024.217.575

formed through thermal annealing and laser irradiation using the in situ method remains an important yet underexplored area of research.

2. Experimental methods

Thin films of GST were fabricated via direct current (DC) ion-plasma sputtering at room temperature, employing a stoichiometric target [4,17]. The key parameters of the film preparation process were adjusted to yield films with an amorphous structure and a composition matching that of the initial target. Specifically, the working gas consisted of argon (99.998%) at a pressure ranging from 0.8 to 1.0 Pa, while the plasma discharge power varied from 50 to 70 W. The distance between the target and the substrate was maintained at 7 cm. Films with thicknesses of 90 nm and 271 nm were deposited onto substrates at room temperature, with quartz and single-crystal silicon (c-Si) serving as the substrates, fixed onto a substrate holder. The average size of the substrates was 1x1.5 cm. To assess the elemental composition, morphology, and thickness of the thin films, energy-dispersive analysis (EDA) and scanning electron microscopy (SEM) were employed using a Quanta 3D 200i complex. Film thickness was determined by scanning of a transverse cleavage of a GST film deposited on a crystalline silicon substrate.

Subsequently, isothermal annealing of the as-prepared GST films was conducted in an argon atmosphere. The temperature of the samples was monitored using a copper-constantan thermocouple (accuracy: ±0.5 °C) at a heating rate of 2°C/min, and maintained constant at T=350°C for 30 minutes.

As an alternative to thermal annealing, GST films underwent annealing via laser irradiation. Laser treatment was carried out utilizing a He-Ne gas laser with a wavelength of 633 nm. Signal acquisition was conducted in the 180° reflection mode via the excitation channel employing a 100x lens. A 1800/500 diffraction grating with a spectral resolution of 1 cm^{-1} was employed, and the CCD detector was cooled to -65°C to minimize noise. The diameter of the laser spot on the sample was approximately 2 μm, with a frequency registration error of ±1 cm^{-1}. Spectral analysis was performed using the OriginPRO 9.1 software.

3. Results and discussion

Figures 1 and 2 display the energy dispersive spectra, the composition of GST films, and SEM images of the transverse cleavage of c-Si/GST film structures. The composition of the as-deposited GST films is presented in the table adjacent to the energy-dispersive spectra. The almost stoichiometric ratio of atoms in the as-deposited GST films with thicknesses of 90 and 271 was confirmed by EDX analysis.

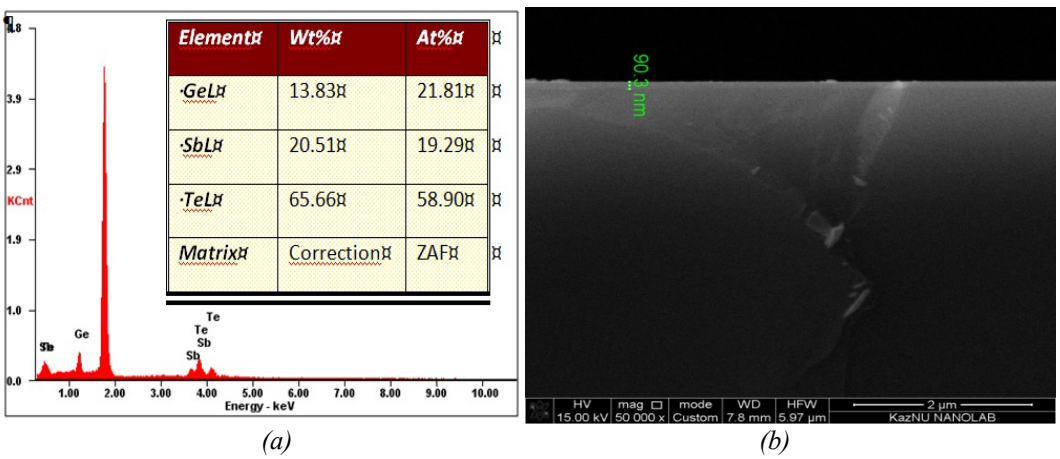

(a) *(b)*

Fig. 1. The energy-dispersive spectrum and chemical composition of a GST film with a thickness of 90.3 nm (a), SEM image of a transverse cleavage of a GST film deposited on a crystalline silicon substrate (b).

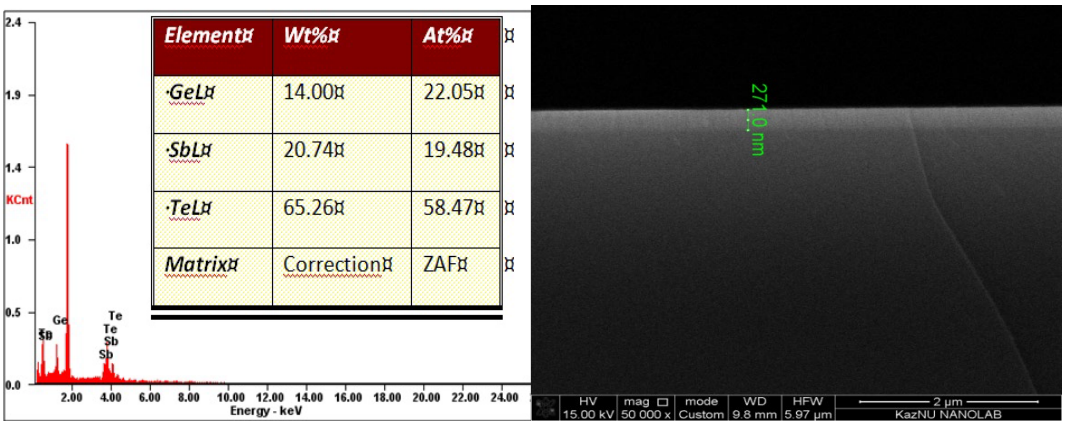

(a) *(b)*

Fig. 2. The energy-dispersive spectrum and chemical composition of a GST film with a thickness of 271 nm (a), SEM image of a transverse cleavage of a GST film deposited on a crystalline silicon substrate (b).

The normalized Raman spectra of GST films, recorded in situ under laser radiation, are presented in Figure 3. For films with an amorphous structure, the spectrum typically features a single peak at 153-155 cm^{-1}. This peak originates from the vibrations of the homopolar Sb–Sb bonds within the Sb_2Te_3 units [18,19]. After 30 seconds of exposure to laser irradiation at a power of 0.81 mW, the 90 nm thick GST film remains entirely amorphous, as shown by the blue line in Figure 3a. In contrast, the 271 nm thick GST film transitions to an fcc state, indicated by the red line in Figure 3b, and exhibits a distinctive peak at 124 cm^{-1}. This peak is likely due to the vibrations of the polar covalent bonds in the $GeTe_4$ and $SbTe_3$ units [20-25]. The Raman spectra of the 90 nm film also shows a slightly noticeable peak at 124 cm^{-1} when the laser intensity hits 1.1 mW, which suggests the formation of a fcc state in it. Further increasing the laser power to 1.27 mW and its exposure time to 30 s leads to an increase in the intensity of this peak, as well as to shift to shorter wavelengths. Two other, less intense peaks can be observed in the films' Raman spectra at 138 cm^{-1} and 160 cm^{-1}. The (Te2)Sb(Te2) complex's Sb-Sb bond vibrations are responsible for the peaks. [18,19].

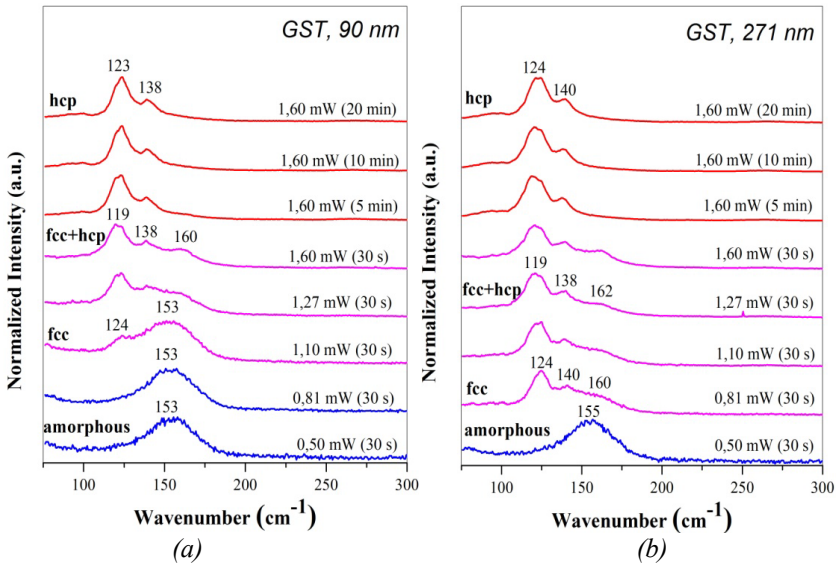

(a) *(b)*

Fig. 3. GST films' Normalized Raman spectra under laser radiation with different power and duration.

The Raman spectra is characteristic of the metastable fcc structure of GST films. Finally, when the laser power reaches 1.60 mW, in the Raman spectrum the intensity of the hexagonal peak increases significantly and takes a stable position at 123-124 cm^{-1}, and an additional low-intensity peak is observed in the region of 138-140 cm^{-1} (Fig. 3 a,b brown lines). The GST films structure transforms from the metastable fcc state to the crystalline hcp state. The similar structural transitions of GST films under laser irradiation were observed in a number of works [26,27].

It was not possible to trace the dynamics of changes in the local structure during thermal annealing using Raman spectra measurements. Thus, for thermally annealed films, measurements of Raman spectra were carried out only in the initial amorphous and final crystallized states. In order to compare, Raman spectra of thin GST films, subjected to thermal and laser annealing, are combined on Fig. 4 a,b. Two distinctive peaks at 121 cm^{-1} and 141 cm^{-1} in the films' Raman spectra indicate that the as-prepared GST films have completely crystallized after 30 minutes of isothermal annealing at T = 350°C. (Fig. 4a,b green line).

From Figures 4 a,b it is clear that the width and intensity of the peaks subjected to laser annealing for both films with thicknesses of 90 and 271 nm are different from those for thermally annealed films of the same thicknesses.

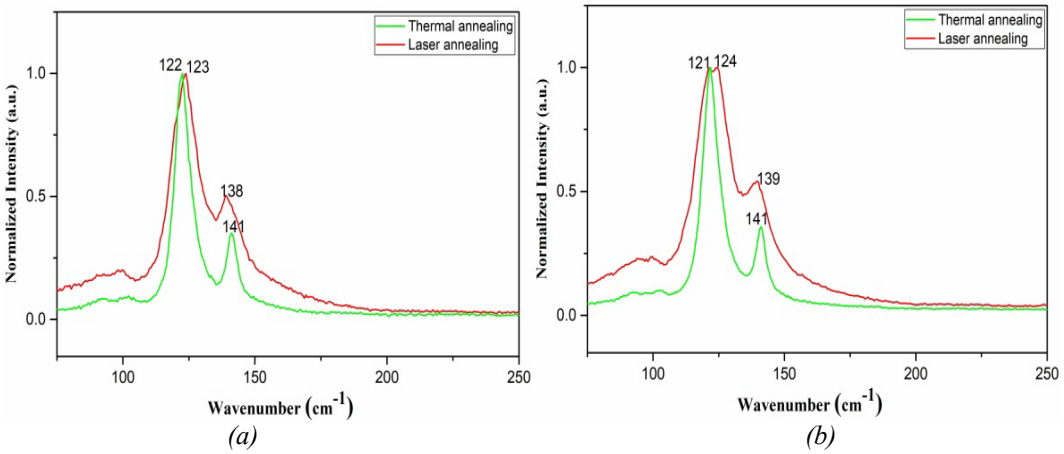

Fig. 4. A comparison between the GST films' Raman spectra with thicknesses of a) 90 nm and b) 271 nm crystallized using thermal and laser annealing.

Raman spectra were subjected to peak fitting via Gaussian deconvolution. The resulting approximation are shown in Fig. 5 and 6, their full width half maximum (FWHM) are listed in Table 1.

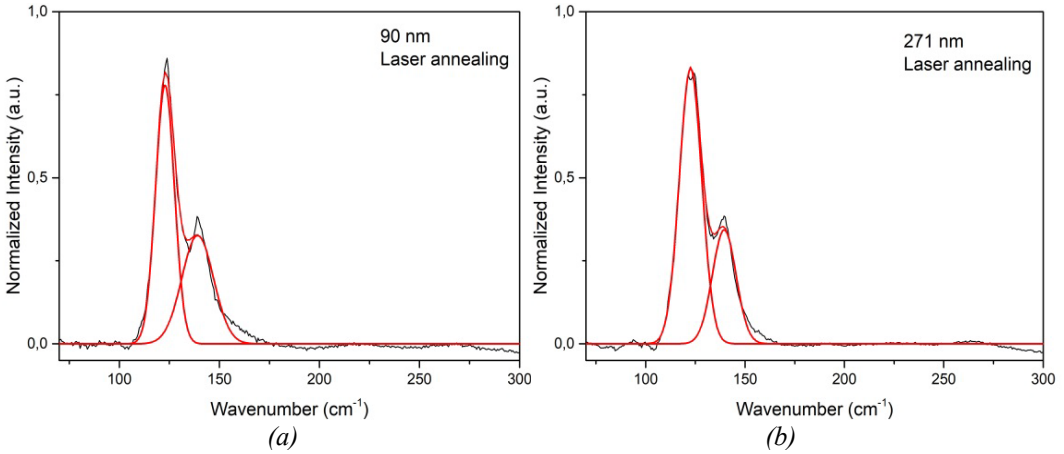

Fig. 5. The Raman spectra of crystalline (hcp state) GST thin film with different thickness (laser annealing): black line; the film's Gaussian distribution-corresponding Raman spectrum: red line.

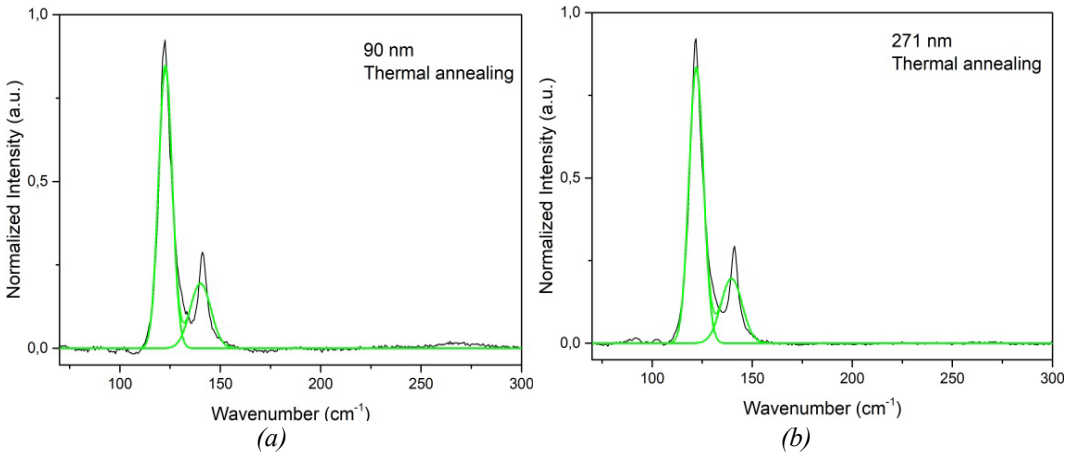

Fig. 6. The Raman spectra of crystalline (hcp state) GST thin film with different thickness (thermal annealing): black line; the film's Gaussian distribution-corresponding Raman spectrum: green line.

Table 1. Fitting results.

Sample	Peak Index	FWHM, (cm^{-1})
90 nm, Amorphous	-	33
90 nm, Laser annealing	1	12
	2	13
90 nm, Thermal annealing	1	8
	2	13
271 nm, Amorphous	-	32
271 nm, Laser annealing	1	13
	2	14
271 nm, Thermal annealing	1	9
	2	13

Table 1 illustrates that the FWHM of the main first peak of GST films significantly decreases upon heat and laser annealing, which causes the films to crystallize. Thus, the FWHM of amorphous films with thicknesses of 90 nm and 271 nm was 33 cm^{-1} and 32 cm^{-1}, respectively. As a result of laser annealing, the first FWHM peak value became approximately 12 cm^{-1} and 13 cm^{-1} for 90 nm and 271 nm films, respectively. Thermal annealing reduced the first FWHM peak value to 8 cm^{-1} and 9 cm^{-1} for films with thicknesses of 90 nm and 271 nm, respectively.

Raman spectra offer plenty of information on the sample's phase and chemical composition, cluster sizes, and other characteristics. While the FWHM of Raman spectra peak is an indicator of crystallinity degree of samples [28-31]. GST films crystallinity degree dropping under laser irradiation (method of spectrum registration in situ) with an increase in their thickness can be associated both with the chemical disorder of the structure under laser irradiation [32] and with the edge effect of laser radiation scattering in the films [33]. The latter assumption is supported by the values of optical transmittance (T) and the effective depth to which laser radiation penetrated into as-prepared films ($d_{eff}=1/\alpha$, here α equal to absorption coefficient). At a laser radiation wavelength of 633 nm, T is 24 and 7%, and d_{eff} is 66 and 40 for the films with thickness of 90 and 271 nm, respectively. It should be noted that different values of d_{eff} correspond to the size effect on the optical characteristics of less than 100 nm-thick GST films, as indicated in [4].

4. Conclusions

Comparative studies of the structure of crystalline thin films of different thickness of phase-alternating composition GST, crystallized by thermal annealing and laser radiation in the process of recording Raman spectra in situ (laser annealing), have been carried out. Using direct current ion-plasma sputtering, films with thicknesses of 90 and 271 nm were produced.

It was found that the crystalline state of all annealed films corresponds to a hexagonal close-packed structure; however the degree of crystallinity of their structure depends on the crystallization method. Moreover, in thermally annealed films, the degree of crystallinity of the structure does not depend on their thickness and is noticeably higher than that in films annealed by laser radiation. While the degree of crystallinity of the film structure during laser annealing noticeably decreases with increasing film thickness. The differences in the GST films' crystallinity degree annealed by different methods are apparently associated with the edge effect of laser radiation scattering in laser annealed films, as well as with the chemical disordering of the films structure.

Acknowledgments

We are grateful to Nazim Guseinov and Renata Nemkayeva of the Al-Farabi Kazakh National University for their assistance with the SEM measurement and the Raman spectroscopic measurement, respectively.

References

[1] Matsunaga, T., Yamada, N. (2004), Japanese journal of applied physics, 43(7S), 4704; https://doi.org/10.1143/JJAP.43.4704

[2] Raoux, S., Burr, G. W., Breitwisch, M. J., Rettner, C. T., Chen, Y. C., Shelby, R. M., Lam, C. H. (2008). IBM Journal of Research and Development, 52(4.5), 465-479; https://doi.org/10.1147/rd.524.0465

[3] Burr, G. W., Breitwisch, M. J., Franceschini, M., Garetto, D., Gopalakrishnan, K., Jackson, B., Shenoy, R. S. (2010). Journal of Vacuum Science & Technology B, 28(2), 223-262; https://doi.org/10.1116/1.3301579

[4] Sultanbekov, S., Prikhodko, O., Almas, N. (2023), Chalcogenide Letters, 20(7); https://doi.org/10.15251/CL.2023.207.487

[5] Sultanbekov, S., Aldongarov, A., Almas, N. (2023, July), 2023 IEEE 23rd International Conference on Nanotechnology (NANO) (pp. 1-6). IEEE; https://doi.org/10.1109/NANO58406.2023.10231170

[6] Sultanbekov, S., Prikhodko, O., Muratov, D., Almas, N. (2023), Journal of Non-Crystalline Solids, 619, 122544; https://doi.org/10.1016/j.jnoncrysol.2023.122544

[7] Behera, J. K., Wang, W., Zhou, X., Guan, S., Weikang, W., Shengyuan, Y. A., Simpson, R. E. (2020), Journal of Materials Science & Technology, 50, 171-177; https://doi.org/10.1016/j.jmst.2020.03.016

[8] Bala, N., Khan, B., Singh, K., Singh, P., Singh, A. P., Thakur, A. (2023), Materials Advances, 4(3), 747-768; https://doi.org/10.1039/D2MA01047J

[9] Yamada, N., Matsunaga, T. (2000), Journal of applied physics, 88(12), 7020-7028; https://doi.org/10.1063/1.1314323

[10] Krusin-Elbaum, L., Cabral, C., Chen, K. N., Copel, M., Abraham, D. W., Reuter, K. B., Deline, V. R. (2007), Applied physics letters, 90(14); https://doi.org/10.1063/1.2719148

[11] Privitera, S., Bongiorno, C., Rimini, E., Zonca, R., Prirovano, A., Bez, R., Mijiritskii, A. (2004). Advanced Data Storage Materials and Characteriztion Techniques.

[12] Chen K.N., Krusin-Elbaum L., Cabral Jr. C., Lavoie C., Sun J., Rossnagel S. Non-Volatile

Semiconductor Memory Workshop. NVSMW-2006. -P. 97−98.

[13] Leervard Pedersen T.P., Kalb J., Njoroge W.K., Wamwangi D., Wuttig M., Spaepen F., Appl. Phys. Lett. -2001. -Vol. 79, Issue 22. -P. 3597−3599; https://doi.org/10.1063/1.1415419

[14] A. A. Sherchenkov, S. A. Kozyukhin, E. V. Gorshkova, J. Optoelectron. Adv. M. **11**(1), 26 (2009).

[15] Olson J.K., Li H., Taylor P.C., J. Ovonic Research. -2005. -Vol. 1. -P. 1−6.

[16] Kalb J., Spaepen F., Wuttig M., J. Appl. Phys. -2003.-Vol. 93. -P. 2389−2393; https://doi.org/10.1063/1.1540227

[17] Zhakiyev, N., Tynyshtykbayev, K., Norem, J., Insepov, Z. (2019), Journal of Physics D: Applied Physics, 53(1), 015503; https://doi.org/10.1088/1361-6463/ab431d

[18] Jackson K., Briley A., /Phys.Rev.B:Condens.Matter.-1999.- Vol.60. -P.22; https://doi.org/10.1103/PhysRevB.60.R14985

[19] Shalini A., Liu Y., Katmis F., Braun W., Srivastava G. P., Hicken R. J., J.Appl.Phys.-2015.-Vol.117. -P.025306; https://doi.org/10.1063/1.4905617

[20] Němec, P., Nazabal, V., Moréac, A., Gutwirth, J., Beneš, L., Frumar, M. (2012), Materials Chemistry and Physics, 136(2-3), 935-941; https://doi.org/10.1016/j.matchemphys.2012.08.024

[21] Kozyukhin, S., Vorobyov, Y., Sherchenkov, A., Babich, A., Vishnyakov, N., Boytsova, O. (2016), Physica Status Solidi A, 213(7), 1831-1838; https://doi.org/10.1002/pssa.201532930

[22] Xu, Z., Chen, C., Wang, Z., Wu, K., Chong, H., Ye, H. (2018), RSC advances, 8(37), 21040-21046; https://doi.org/10.1039/C8RA01382A

[23] Andrikopoulos, K. S., Yannopoulos, S. N., Kolobov, A. V., Fons, P., Tominaga, J. (2007), Journal of Physics and Chemistry of Solids, 68(5-6), 1074-1078; https://doi.org/10.1016/j.jpcs.2007.02.027

[24] Kozyukhin, S., Lazarenko, P., Vorobyov, Y., Baranchikov, A., Glukhenkaya, V., Smayev, M., Sigaev, V. (2019), Optics & Laser Technology, 113, 87-94; https://doi.org/10.1016/j.optlastec.2018.12.017

[25] Andrikopoulos, K. S., Yannopoulos, S. N., Kolobov, A. V., Fons, P., Tominaga, J. (2007), Journal of Physics and Chemistry of Solids, 68(5-6), 1074-1078.

[26] Prikhodko, O. Y., Ismailova, G. A., Zhakypov, A. S., Kolobov, A. V., Turmanova, K. N., Nemkaeva, R. R., Peshaya, S. L. (2023), Journal of Electronic Materials, 52(4), 2492-2498; https://doi.org/10.1016/j.jpcs.2007.02.027

[27] Du, J., Mu, Z., Li, L., Li, J. (2021), Optics and Laser Technology, 144, 107393; https://doi.org/10.1016/j.optlastec.2021.107393

[28] Patil, A., Le-Friec, Y., Sandrini, J., Simola, R., Boivin, P., Dubois, E., Robillard, J. F. (2022, September), 2022 28th International Workshop on Thermal Investigations of ICs and Systems (THERMINIC) (pp. 1-5). IEEE; https://doi.org/10.1109/THERMINIC57263.2022.9950662

[29] Zallo, E., Dragoni, D., Zaytseva, Y., Cecchi, S., Borgardt, N. I., Bernasconi, M., Calarco, R. (2021), Physica Status Solidi (RRL)-Rapid Research Letters, 15(3), 2000434; https://doi.org/10.1002/pssr.202000434

[30] Zallo, E., Cecchi, S., Boschker, J. E., Mio, A. M., Arciprete, F., Privitera, S., Calarco, R. (2017), Scientific Reports, 7(1), 1466; https://doi.org/10.1038/s41598-017-01502-z

[31] Lotnyk, A., Dankwort, T., Hilmi, I., Kienle, L., Rauschenbach, B. (2019), Nanoscale, 11(22), 10838-10845; https://doi.org/10.1039/C9NR02112D

[32] Du, J., Mu, Z., Li, L., Li, J. (2021), Optics and Laser Technology, 144, 107393; https://doi.org/10.1016/j.optlastec.2021.107393

[33] Wang, K., Wamwangi, D., Ziegler, S., Steimer, C., Wuttig, M. (2004), Journal of applied physics, 96(10), 5557-5562; https://doi.org/10.1063/1.1803612